Supporting Information

Lewis et al. 10.1073/pnas.1513773113

SI Experimental Procedures

Neurophysiological Recording Techniques and Signal Preprocessing. Neuronal recordings were made from two left hemispheres in two monkeys through a micromachined 252-channel electrocorticogram-electrode array with 1-mm-diameter contacts spaced by 2.5–3 mm and implanted subdurally (1–4). Electrode impedance was ~3 kΩ at 1 kHz. The reference electrode was a silver ball places over the contralateral visual cortex. The common recording reference was removed through calculating the bipolar derivation before any further processing. Briefly, a 6.5 × 3.4-cm craniotomy over the left hemisphere in each monkey was performed under aseptic conditions with isoflurane/fentanyl anesthesia. The dura was opened, and the ECoG was placed directly onto the brain under visual control. Several high-resolution photographs were taken before and after placement of the ECoG for later coregistration of ECoG signals with brain regions. After ECoG implantation, both the bone and the dura flap were placed back and secured in place. ECoG electrodes covered numerous brain areas, including parts of areas V1, V2, V4, and TEO. As mentioned in the main text, retinotopic mapping revealed two contiguous maps of space: one behind the lunate sulcus for areas V1/V2 and another one between the lunate and the superior temporal sulcus for areas V4/TEO. For simplicity, we will refer to ECoG sites in the V1/V2 map as V1 and to sites in the V4/TEO map as V4. After a recovery period of ~3 wk, we started neuronal recordings. Signals obtained from the electrode grid were amplified 20 times by eight Plexon headstage amplifiers and then low-pass filtered at 8 kHz and digitized at 32 kHz by a Neuralynx Digital Lynx system. LFP signals were obtained by low-pass filtering at 200 Hz and down-sampling to 1 kHz. Power line artifacts were removed by digital notch filtering. The actual spectral data analysis included spectral smoothing that rendered the original notch invisible. The data used for the analysis presented in this manuscript are available to interested parties by contacting the authors.

Visual Stimulation. Stimuli and behavior were controlled by the software CORTEX. Stimuli were presented on a cathode ray tube monitor at 120 Hz noninterlaced. When the monkey touched a bar, a gray fixation point appeared at the center of the screen. When the monkey brought its gaze into a fixation window around the fixation point (0.85 radius in monkey K; 1 radius in monkey P), a prestimulus baseline of 0.8 s started. If the monkey's gaze left the fixation window at any time, the trial was terminated.

Several sessions (either separate or after attention-task sessions) were devoted to the mapping of receptive fields, using 60 patches of drifting grating, as illustrated in Fig. 1*B*. Gratings were circular black and white sine waves, with a spatial frequency of 3 cycles/° and a speed of 0.4°/s presented for 1.1 s. Stimulus diameter was scaled between 1.2° and 1.86° to account for cortical magnification factor. Receptive field positions were stable across recording sessions (see figure S1*D* of ref. 12).

Data Analysis General. We calculated local bipolar derivatives, i.e., differences (sample-by-sample in the time domain) between LFPs from immediately neighboring electrodes. We refer to the bipolar derivatives as sites. Bipolar derivation removes the common recording reference, which is important when analyzing power correlations and/or coherence. In this scheme, neighboring sites have an electrode in common. We limited our analysis to interareal site pairs, which never have a common electrode. Subsequently, per site and individual epoch, the mean was subtracted, and then, per site and session, the signal was normalized by its SD. These normalized signals were pooled across sessions with identical stimulus and task, unless indicated otherwise. To select solely visually selective recording sites, an ANOVA was computed across frequencies (Fig. 1*C* and Fig. S1*B*).

Time series of band-limited power were computed for each trial by filtering the data with a one-pass, causal Butterworth filter of order 2. We used a one-pass filter to avoid stimulation-related activity from contaminating epochs of passive fixation. Qualitatively similar results were found by using shorter time periods and a two-pass filter. Data were filtered into 185 frequency bands with center frequencies between 2 and 200 Hz. We used different pass bands in computing the analysis to confirm the robustness of the results, and in the results presented here, we chose three different pass bands for three different groups of center frequencies (CFs): 3 Hz for low (CF = 2–11 Hz), 6 Hz for medium (CF = 13–53 Hz), and 15 Hz for high (CF = 59–200 Hz). After filtering, we calculated the Hilbert transform and took the absolute value of the analytic signal. All fixation trials were then concatenated into a pseudocontinuous time series for calculation of the interareal correlation coefficient.

Statistical Testing. The false-positive rate was controlled by our statistical testing procedure as follows. To compute significance thresholds for both frequency planes and line spectra, surrogate data were used which broke the spatial pattern of interareal interaction but kept all other features (e.g., the distribution and interareal pattern of signal correlations and the distribution of intrinsic correlation and coherence) unchanged. Surrogate data were generated by creating 1,000 random pairings of interareal site pairs and then computing the correlation across site pairs, between the signal correlations and (*i*) the noise correlation, (*ii*) the spontaneous correlation, (*iii*) the coherence, and (*iv*) the GC influences. Each realization of the randomized structure resulted in a distribution of correlation coefficients. In all cases, we set our threshold for significance across all tests at $P < 0.05$. In the case of noise correlation, because this came from the same dataset as the index for stimulus selectivity, we used an omnibus-based multiple comparison correction (5, 6). In this case, we retained the maximum surrogate correlation coefficient (absolute value) across all combinations of frequencies and corrected our empirical distributions by thresholding at the $P < 0.05$ level from this distribution of surrogate maxima. In the other cases, because the analysis was from independent data, we used the less conservative false discovery rate (FDR) correction (7). To compute FDR corrections, we retained all correlation values across all randomizations in a single distribution and took our significance threshold from the $P < 0.05$ level of this complete distribution.

1. Rubehn B, Bosman C, Oostenveld R, Fries P, Stieglitz T (2009) A MEMS-based flexible multichannel ECoG-electrode array. *J Neural Eng* 6(3):036003.
2. Bosman CA, et al. (2012) Attentional stimulus selection through selective synchronization between monkey visual areas. *Neuron* 75(5):875–888.
3. Brunet NM, et al. (2014) Stimulus repetition modulates gamma-band synchronization in primate visual cortex. *Proc Natl Acad Sci USA* 111(9):3626–3631.
4. Brunet N, et al. (2015) Visual cortical gamma-band activity during free viewing of natural images. *Cereb Cortex* 25(4):918–926.
5. Maris E, Schoffelen J-MM, Fries P (2007) Nonparametric statistical testing of coherence differences. *J Neurosci Methods* 163(1):161–175.
6. Nichols TE, Holmes AP (2002) Nonparametric permutation tests for functional neuroimaging: A primer with examples. *Hum Brain Mapp* 15(1):1–25.
7. Genovese CR, Lazar NA, Nichols T (2002) Thresholding of statistical maps in functional neuroimaging using the false discovery rate. *Neuroimage* 15(4):870–878.

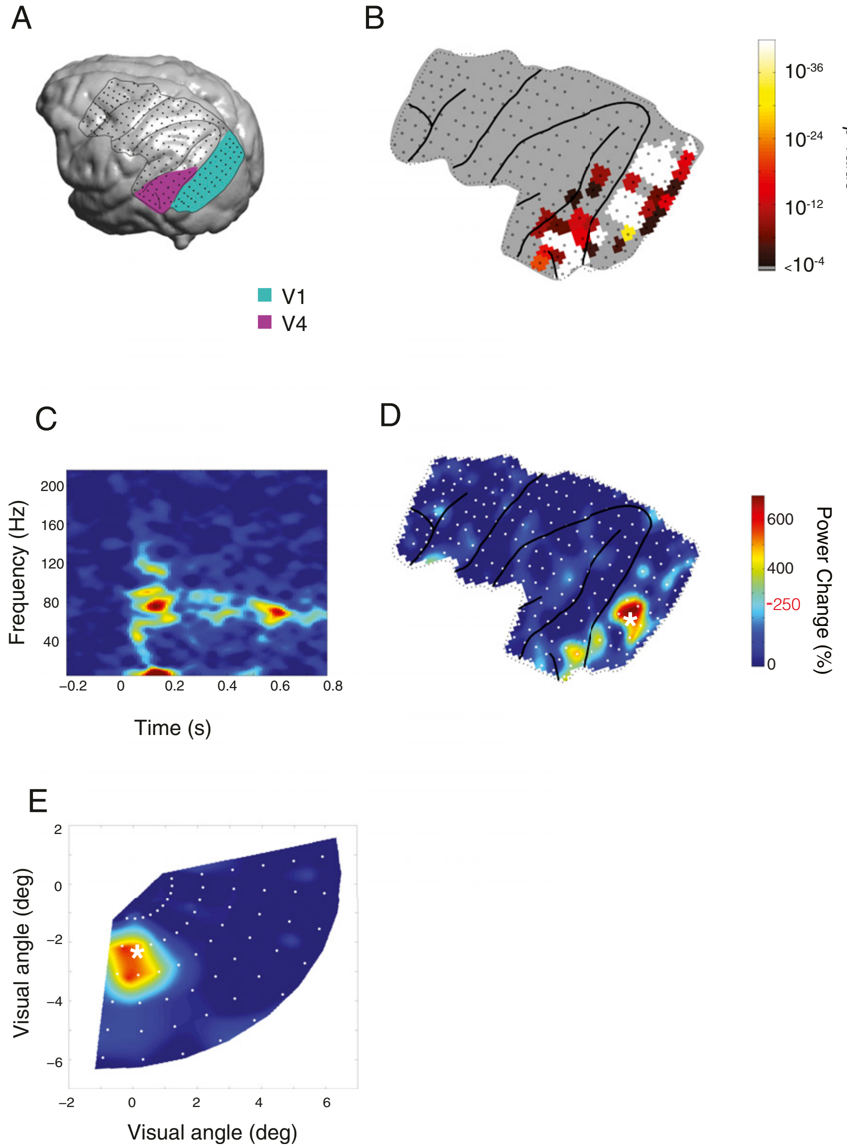

Fig. S1. High-density ECoG layout and retinotopic selectivity. (*A*) Rendering of the brain of monkey K with ECoG overlaid. Lines indicate the covered area with the major sulci. Dots indicate the 218 bipolar electrode derivations. Sites considered as lying in areas V1 and V2 are highlighted in green and those in areas V4 and TEO are highlighted in purple. (*B*) Selectivity of all ECoG sites for stimulus position based on stimulus-induced power in all frequency bands. (*C–E*) Example average response to stimulation at the position marked in Fig. 1*B*. (*C*) Time–frequency plot at the site marked by a star in *D*. Topographic plot of induced gamma power (80–95 Hz) for each ECoG site. (*E*) Induced gamma band response across all positions for the site marked in *D*. Color bar is the same for *C–E*; red line and value next to color bar indicate significance.

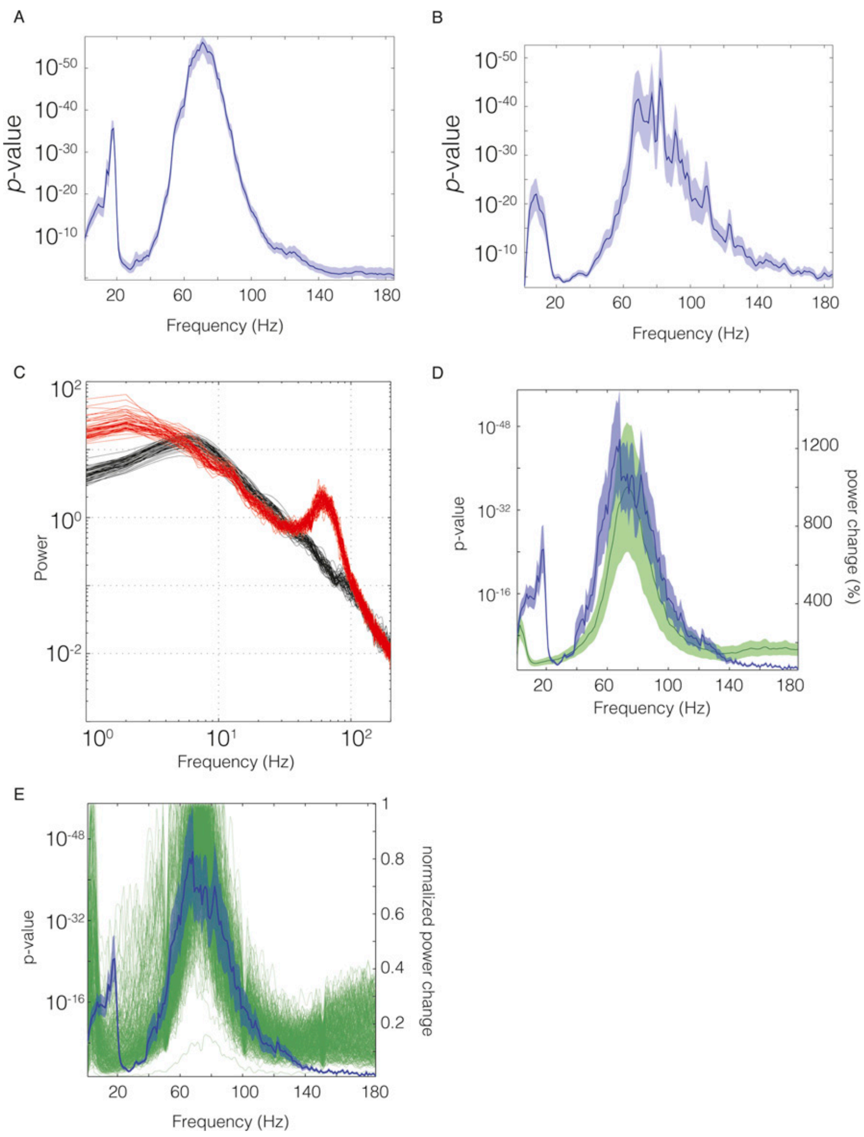

Fig. S2. Selectivity of position-tuned sites as a function of frequency for each monkey: (*A*) monkey P and (*B*) monkey K. Mean across visual channels in dark and variance around the mean in shaded region. (*C*) Spectrum of LFP power for prestimulus (black) and poststimulus (red) periods computed on each individual trial for the stimulus position and recording site shown in Fig. 1*E*. (*D*) Comparison of the stimulus position selectivity of the power as a function of frequency (blue curves) and the stimulus-induced relative power increase (green curves) for both monkeys. (*E*) Same as *D* but showing the relative power increase for all visually tuned recording sites to their top five stimulus locations for both monkeys.

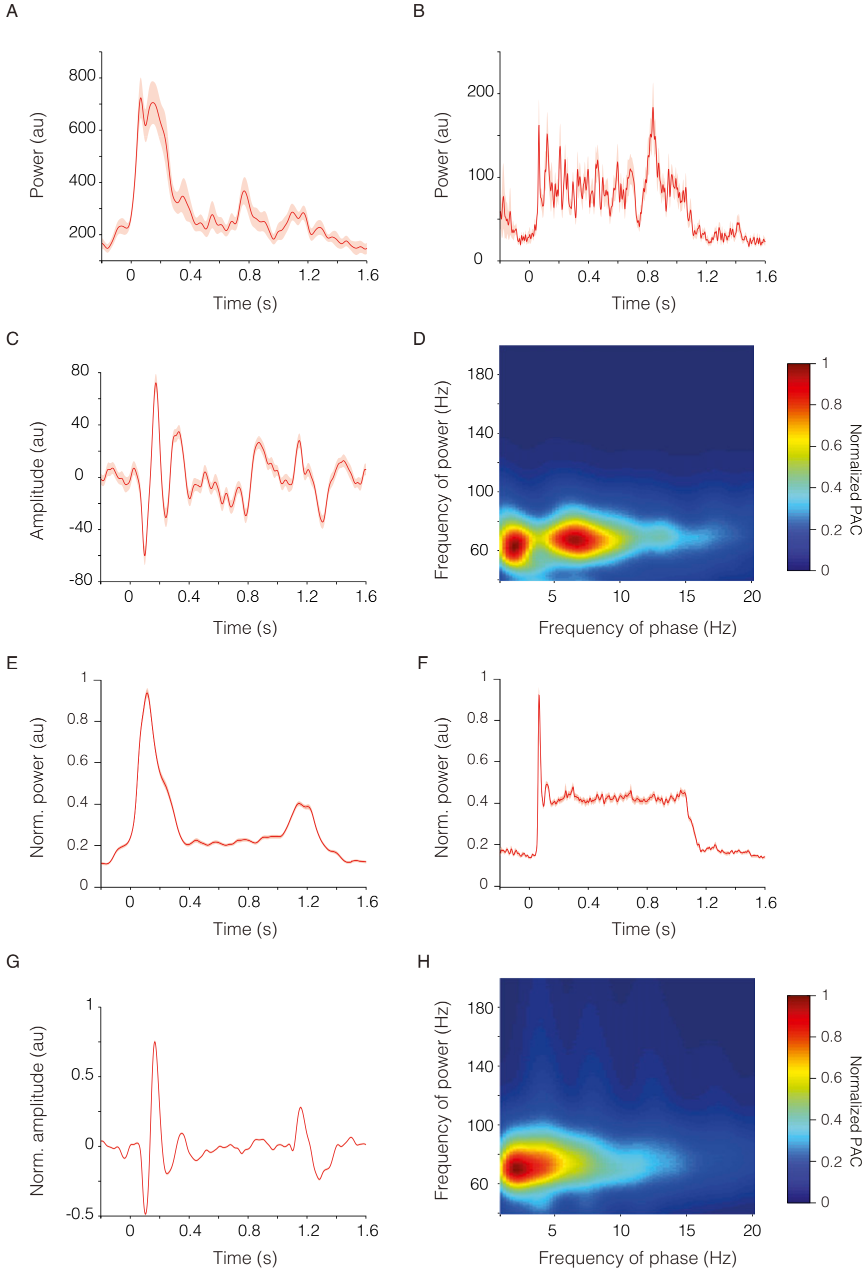

Fig. S3. Low-frequency and gamma-band power and phase-amplitude coupling during visual stimulation. (*A*) Low-pass visual activity for one example site driven by its optimal stimulus as a function of time around stimulus presentation. (*B*) Low-frequency power as in *A*. (*C*) Gamma-band power as in *A*. (*D*) Phase-amplitude coupling between low-frequency phase and high-frequency power during steady-state visual response. (*E–H*) As in *A–D*, but for all visual channels in both monkeys to their respective optimal stimulus.

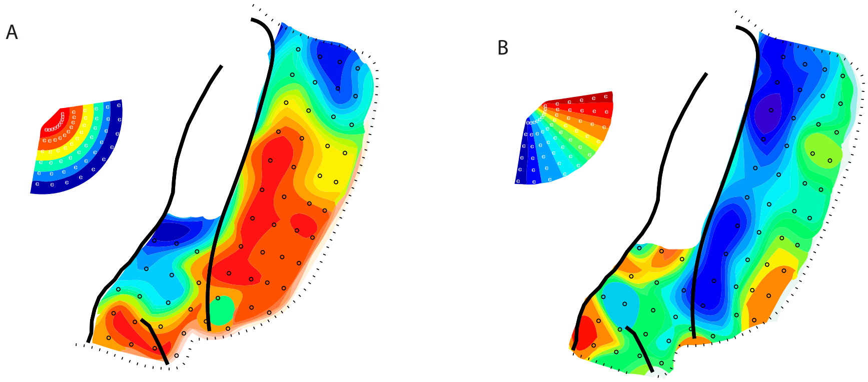

Fig. S4. Retinotopic maps based on gamma-band (80–95 Hz) activity in monkey K. (*A*) Map of eccentricity; each recording site is colored to indicate the mean eccentricity of the five stimuli giving the largest gamma band response. (*B*) Map of elevation; each recording site is colored to indicate the mean elevation as estimated above. *Inset* shows how the 60 stimulus locations are represented across eccentricity and elevation.

PNAS PNAS PNAS

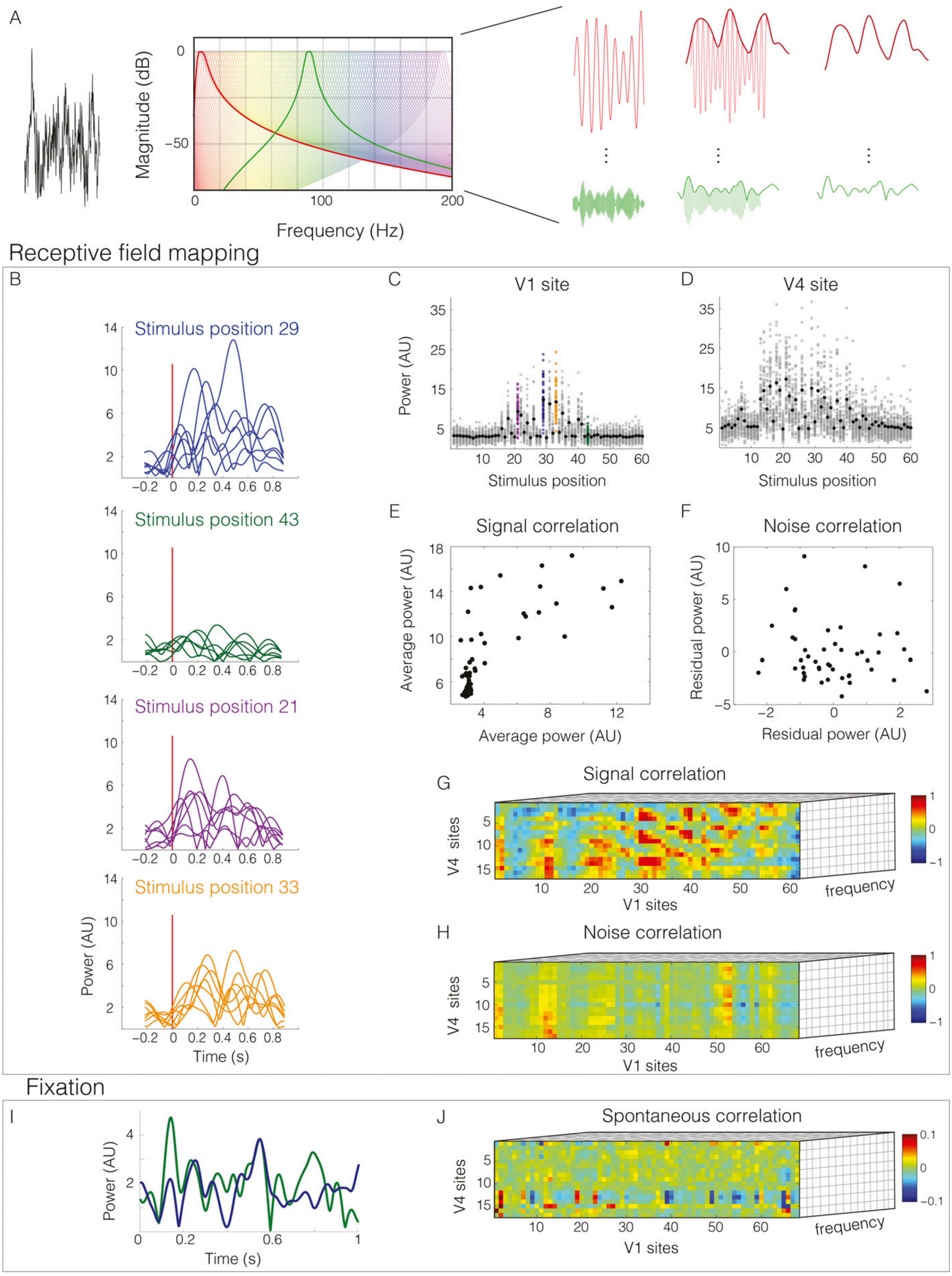

Fig. S5. Analysis pipeline for visual stimulation and passive fixation. (*A*) Signal processing pipeline: raw field potentials (*Left*) were filtered in 185 linearly spaced bands between 2 and 200 Hz (*Center*). The power envelope was extracted from the analytic Hilbert representation (*Right*). Receptive field mapping. (*B*) Example power responses in the gamma band (80–95 Hz) for one V1 site to seven repetitions of visual stimulation at four positions. (*C*) Average (in black) and individual trial (in gray) responses of the same V1 site to all 60 stimulus positions. Positions in *B* shown in the respective color. (*D*) Same as *C* but for an example V4 site. (*E*) The signal correlation for the two sites shown above. (*F*) The noise correlation for the same two sites. Signal (*G*) and noise (*H*) correlations were computed between all pairs of V1–V4 sites for all frequencies of interest. Passive fixation. (*I*) One second of activity in the gamma band for the same V1–V4 sites shown above. (*J*) Spontaneous correlation was computed for all pairs of V1–V4 sites in each frequency of interest.

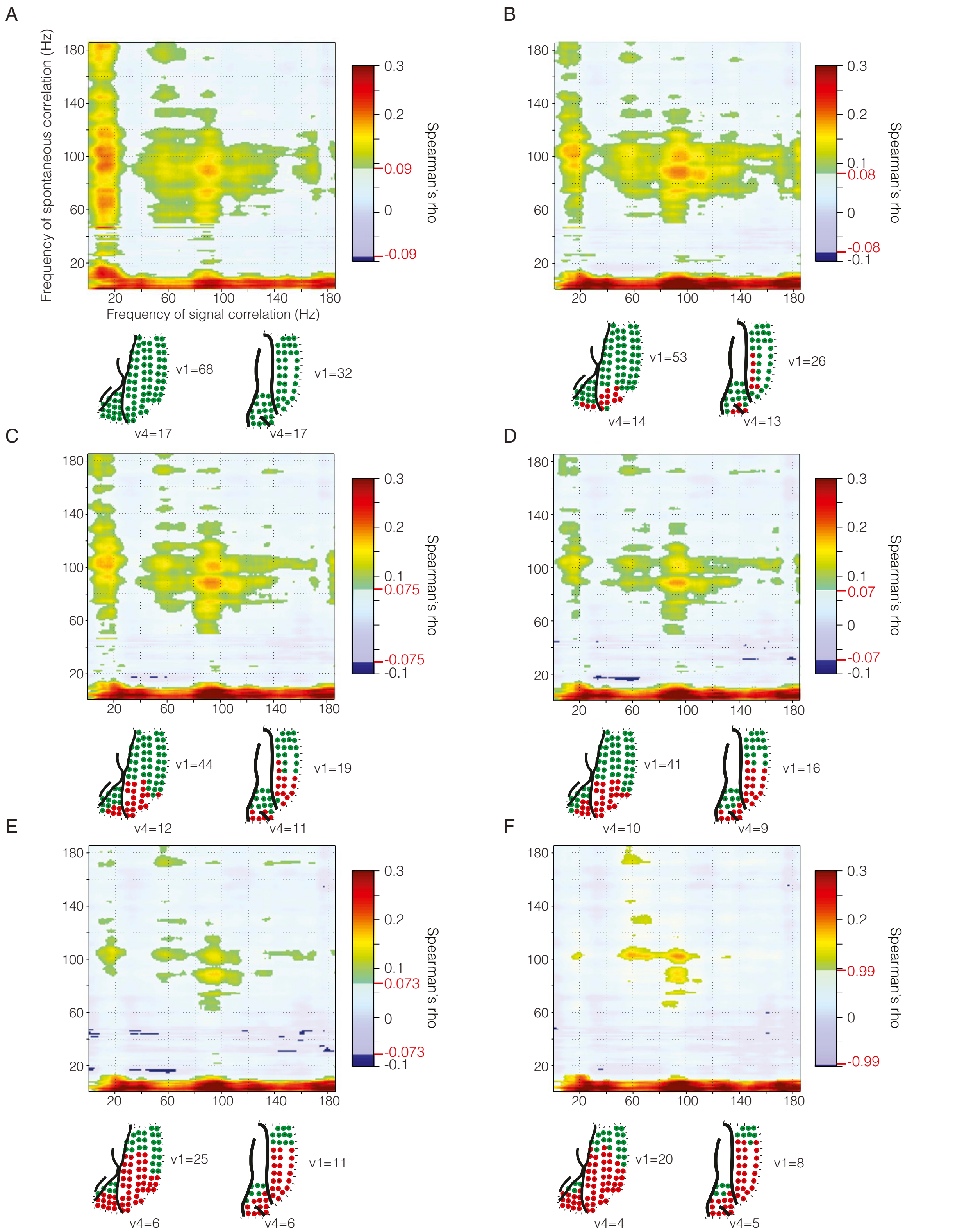

Fig. S6. Spontaneous power correlations after removing parafoveal channels. (*A*) Correlation of spontaneous V1–V4 power correlations and signal correlations for all visual sites. Lower portion shows sites included (in green) and removed (in red). (*B*) As in *A*, but after removing all visual sites with selectivity ≤1°. (*C*) As in *A*, but after removing all visual sites with selectivity ≤1.5°. (*D*) As in *A*, but after removing all visual sites with selectivity ≤2°. (*E*) As in *A*, but after removing all visual sites with selectivity ≤2.5°. (*F*) As in *A*, but after removing all visual sites with selectivity ≤3°.

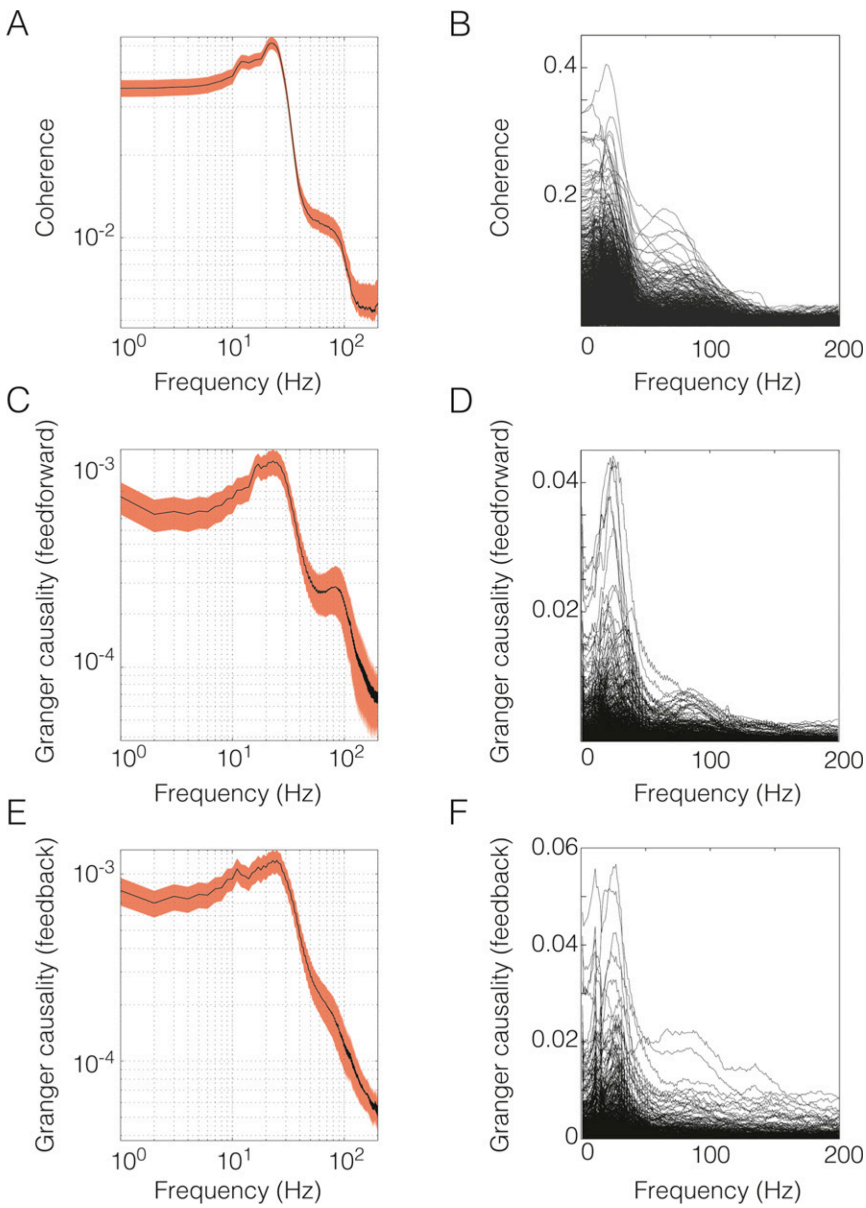

Fig. S7. Spontaneous coherence and GC spectra. (*A*) Log-log plot of coherence between all V1 and V4 pairs for both monkeys during the fixation period. (*B*) Coherence for all V1–V4 pairs during fixation for monkey P. Gamma band activity is visible, although there is no conspicuous gamma activity in the power spectrum for these recording sites (Fig. 5*G*). (*C*) Log-log plot of feed-forward GC between all V1 and V4 pairs for both monkeys during the fixation period. (*D*) Feed-forward GC for all V1–V4 pairs during fixation for monkey P. Gamma band activity is visible, although there is no conspicuous gamma activity in the power spectrum for these recording sites (Fig. 5*G*). (*E*) Log-log plot of feedback GC between all V1 and V4 pairs for both monkeys during the fixation period. (*F*) Feedback GC for all V1–V4 pairs during fixation for monkey P. Gamma band activity is visible, although to a lesser extent than for coherence or feed-forward GC.

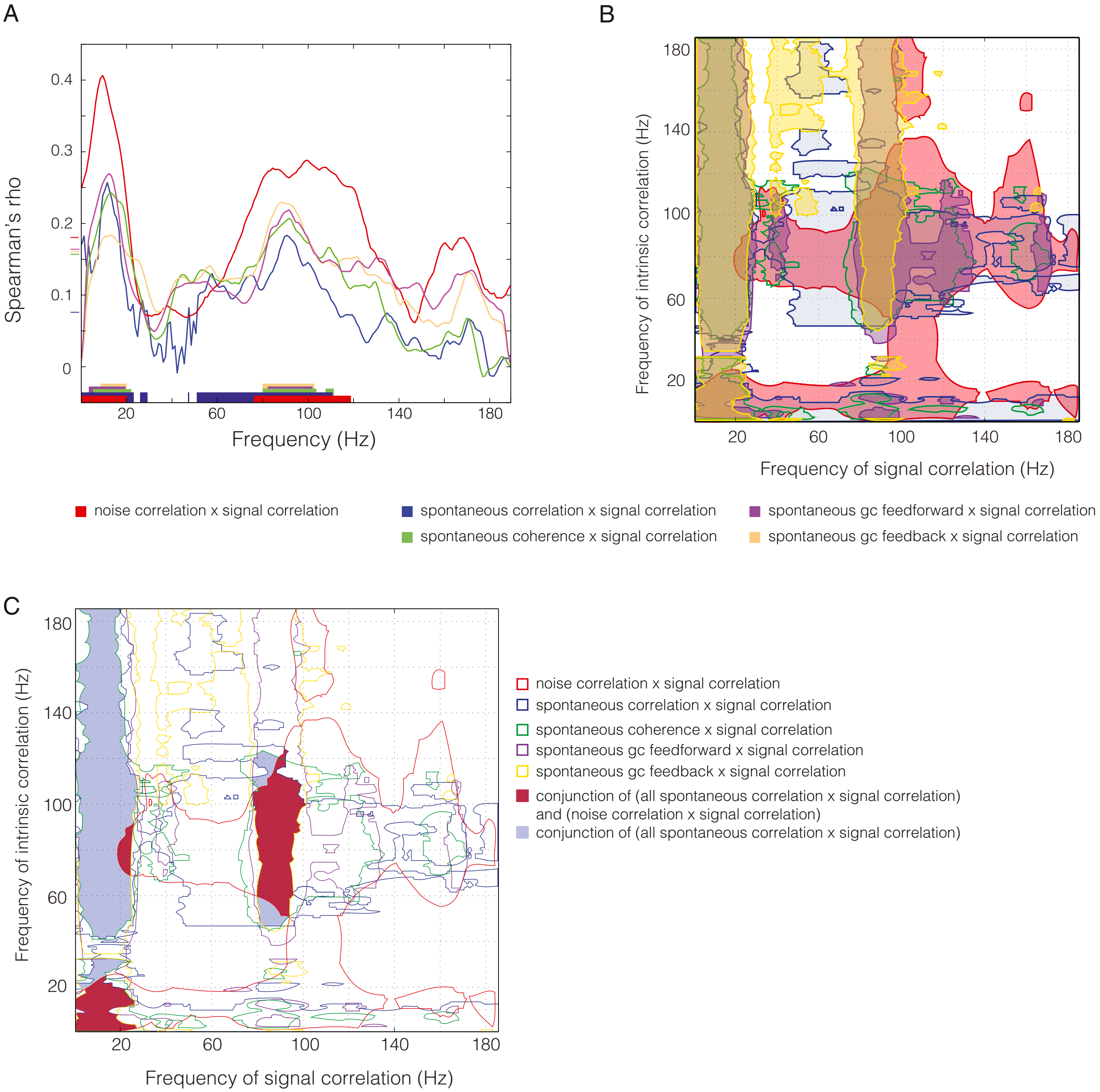

Fig. S8. Comparison of frequency–frequency correspondence of intrinsic and signal correlations. (*A*) Line spectra from the diagonal of each respective frequency–frequency plane. The spectra illustrate the pervasive pattern of correspondence between intrinsic and signal correlations. Noise correlations, spontaneous power correlations, spontaneous coherence, and spontaneous GC all show two regions of correspondence with the pattern of interareal signal correlations. One region is between 8 and 20 Hz and the other is between 80 and 105 Hz. (*B*) Frequency–frequency plots illustrating the consistent pattern of correspondence between intrinsic and signal correlations. Same as in *A*, but for all frequency–frequency pairs. (*C*) Same as in *B*, but highlighting the consistent patterns of frequency–frequency correspondence exhibited by all measures of intrinsic correlation presented here (red regions) and those exhibited by spontaneous correlation (blue regions + red regions). The broadband correspondence observed during spontaneous activity can be seen along with the band-limited components occurring during both stimulation and passive fixation.